International Journal of Speleology	53 (1)	63-73	Tampa, FL (USA)	January 2024

Available online at scholarcommons.usf.edu/ijs

International Journal of Speleology

Official Journal of Union Internationale de Spéléologie

Monitoring air fluxes in caves using digital flow meters

Claudio Pastore [1,2*], Amir Sedaghatkish [1,2] Eric Weber [1], Nicolas Schmid [1], Pierre-Yves Jeannin [1], and Marc Luetscher [1]

[1]Swiss Institute for Speleology and Karst Studies (SISKA), Rue de la Serre 68, 2300 La Chaux-de-Fonds, Switzerland
[2]Université de Neuchâtel, Avenue du 1er-Mars 26, 2000 Neuchâtel, Switzerland

Abstract: Precise measurements of airflow within caves are increasingly demanded to assess heat and mass transfers and their impacts on the karst environment, including subsurface ecosystems, hydrochemistry of karst water and secondary mineral precipitates. In this study, we introduce a new, low-cost and lightweight device adapted to monitoring air fluxes in caves which addresses the need for reliable measurements, low power consumption, durability and affordability. The device was calibrated in a wind tunnel, showing the high accuracy and precision of the device. Field-related uncertainties were further investigated in a ventilated cave to determine the effect of local airflow conditions on the inferred mass flux. Comparing measured values with a 3-D air velocity distribution modelled on a surveyed cave section suggests that most of the uncertainties in estimating the airflow result from the relative position of the instrument in the streamlines rather than from the accuracy of the device.

Keywords: air flow, cave monitoring, chimney effect, velocity distribution model

Received 27 February 2024; Revised 5 June 2024; Accepted 7 June 2024

Citation: Pastore, C., Sedaghatkish, A., Weber, E., Schmid, N., Jeannin, P.-Y., Luetscher, M., 2024. Monitoring air fluxes in caves using digital flow meters. International Journal of Speleology, 53(1), 63-73. https://doi.org/10.5038/1827-806X.53.1.2500

INTRODUCTION

Accurate measurements of air fluxes in caves are increasingly demanded to quantify heat and mass transfers for their implication on the karst water hydrochemistry (Jeannin et al., 2017) and secondary calcite precipitates (Spötl et al., 2005) as well as for assessing their impact on subsurface ecosystems (Dominguez-Moñino et al., 2021). Because airflow largely controls the cave climate (Luetscher & Jeannin, 2004; Luetscher et al., 2008), quantitative measurements are needed for paleoclimate reconstruction, for assessing habitat evolution (Medina et al., 2023) of numerous specific and often endemic species, and even for carbon cycle estimates (Breecker et al., 2012; Prelovšek et al., 2018; Martin-Pozas et al., 2022), as they control CO_2 concentrations (Kowalczk & Froelich, 2010; Faimon & Lang, 2013; Kukuljan et al., 2021) in the whole volume of carbonate rocks. Some authors relied on airflow monitoring to assess the air energy balance in ventilated caves and its impact on underground ice masses (Luetscher et al., 2008).

Different types of anemometers are available on the market, including 1) analogue anemometers, 2) hotwire anemometers, and 3) ultrasonic anemometers, offering a wide range of costs and quality of measurements. While each of these instruments is suited to specific monitoring ranges, they either have limited resolution and mechanical inertia (1), lack indication of the airflow direction (2) or require a high power supply (2, 3)(Fan et al., 2018; George et al., 2018), although the available technology is constantly improving (Fan et al., 2018; Leoni et al., 2018; Wang et al., 2021). Moreover, cave air drafts could be associated with low speeds (<1 m/s), in particular when the cross-section is large or with a small driving force (e.g., reduced seasonality, small vertical development and/or natural convection cells) (Kukuljan et al., 2021; Gabrovšek, 2023). There, measurements can be affected by instrumental precision and would require high-resolution monitoring with e.g. ultrasonic devices or hot-wire anemometers which ensure high precision and accuracy. However, these instruments are sensitive to cave-specific environmental conditions and their prohibitive costs make them difficult to be installed routinely in remote cave parts. While most of these instruments are designed to be installed outdoors, where climatic conditions are very variable (alternating sunny and rainy days, varying relative humidity and temperatures), others are designed specifically for indoor applications under steady conditions (e.g., in ventilation ducts or for medical purposes). In cave conduits, climatic

*claudio.pastore@isska.ch

conditions are less variable than outside but the condensing environment represents nonetheless an extreme environment for these devices. These climatic conditions can alter the integrity of the collected data during monitoring campaigns whilst extra heating caps require an additional power supply, possibly influencing the cave climate locally.

We have tested several devices in the past, including a highly sensible ultrasonic anemometer. However, during long-term monitoring, most of the instruments did not work properly for several reasons: condensing environment, failure of electronic parts, drifting and untrustable measurements.

Here we test a new, low-cost and lightweight device for the automated monitoring of air fluxes in caves. This analysis aims to find out:

- the suitability of the instrument outside the manufacturer's declared working conditions;
- the uncertainties over the range of potential velocities found in caves;
- a reliable conversion curve between the raw standard litre per minute (SLM) measured by the device into a velocity in meters per second.

Eventually, cave airflow (from now on referred to as volumetric airflow in m^3/s) is derived from the integration of air velocities through a known cross-section. The inferred airflow through a cross-section is, however, subject to uncertainties related to singularities along a cave conduit (e.g., rock chocks and asperities) which can modify the velocity distribution within the conduit (Pastore et al., 2024) and cross-section. This raises the question of the best location to deploy a device to infer a close-to-average airspeed. To address this point, we carried out a numerical simulation of air velocity distributions based on a 3-D lidar scan of a cave conduit. Results were compared with experimental measurements carried out with the digital flowmeter.

MATERIALS AND METHODS

Sensirion SFM3003-300-CE

Originally developed for measuring airflow in a closed system for medical applications, the Sensirion SFM3003-300-CE (from now on SFM) is a digital bidirectional mass flowmeter ready to be implemented on a 3.3 V microcontroller based on an I2C protocol. The device is compact and robust, shows a high data resolution (up to 16 bit) and has low power requirements (typically 3.3 V / ~3.8 mA during measurements). This last point is fundamental in caves, where electrical energy is often limited to batteries which should last as long as possible to ensure continuous data recording. Furthermore, the bidirectional cave airflow is well recognised by the device which records the flow direction as negative or positive values (Fig. 1).

The device measures the flow rate in standard litres per minute (SLM) at standard conditions (T = 20°C and P = 1013 mbar), with a declared accuracy of ±2% of the measured value. The instrument has a calorimetric element sensor based on a micro-electromechanical system (MEMS). The microelements are on a silicon chip, which hosts a micro-heater and an upstream and downstream temperature sensor. The heater generates a thermal field. In the absence of flow, the temperature of the two sensors is equal and the thermal field is symmetric. In the presence of a draft, the instrument determines the thermal asymmetry (oriented as the flow) by measuring the ΔT at the two extremities which produces a measurable signal that is a function of the flow velocity (Monitaro and Domanski, 2023). To check the SFM precision and accuracy, independent calibration was carried out in a wind tunnel at the Swiss Federal Institute of Metrology (METAS).

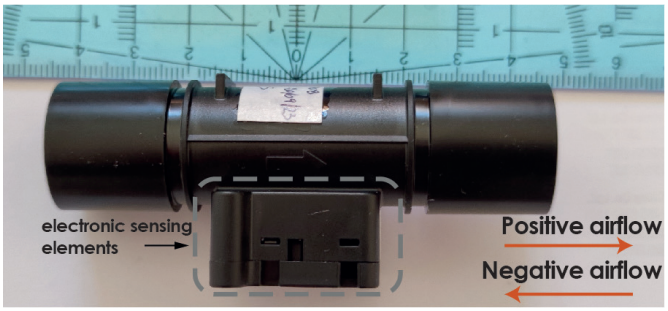

Fig. 1. Sensirion SFM 3003-300 CE. Internal pipe diameter: 3.61 cm.

Calibration test and instrumental reproducibility

The Swiss Federal Institute of Metrology (METAS) hosts a wind tunnel (flow velocity's BIPM ID: EURAMET-M-CH-00000CIJ-1) able to generate air drafts between 0.10 and 50 m/s at extremely high accuracy (Table 1).

Table 1. METAS' uncertainties related to wind velocity measured in the wind tunnel.

Type of instrument	Measuring range	Uncertainty
Anemometers	v = 0.10 – 1.0 m/s	0.02 m/s for v < 1 m/s
	v = 1.0 – 50.0 m/s	2% for v > 1 m/s

The device SFM_SN0708 was clipped on a rod in an open section of the wind tunnel (Fig. 2a, b) and was tested over a range of air velocities between 0.15 and 8 m/s (n = 11). The instrument was calibrated for both directions (at θ = 0° for positive and θ = 180° for negative values) and a rotation experiment was carried out at three different velocities (1.2, 1.6, 5.0 m/s) at θ angles of 10°, 20°, 30°, and 45° from the vertical axis, respectively (Fig. 2c).

The SFM was connected to the laptop through the SEK-Control Center software v.1.38 (Sensirion®, 2024). The data sampling rate ran at 100 Hz and the flow rate was averaged and logged every five measurements. The average (Avg_{SLM}) and the standard deviation (σ_{SLM}) of the measured values (n = 401) were determined for each reference velocity (V_{ref}).

The SFM's absolute error (Err_{abs}) is given by

$$\sqrt{Err_{ref}^{\ 2} + Err_{SFM}^{\ 2}}$$

where Err_{ref} is the error on the reference velocity based on the V_{ref} standard deviation and uncertainty given in Table 1, and Err_{SFM} is the velocity error on SFM measurements inferred as $V_{ref} \times 2\sigma_{SLM} / Avg_{SLM}$.

The reproducibility of the instruments was investigated in the lab at the Suisse Institute for

Speleology and Karst Studies (SISKA) by comparing measurements from two different devices, SFM-1 (SN0501) and SFM-2 (SN0382), with the calibrated reference (SFM_SN0708) at different air velocities. The airflow was generated using a fan mounted on a 1.10 m-long pipe and powered with an adjustable supply. The fan velocity was controlled by eight different voltages between 5 V and 30 V.

Instrumental reproducibility was tested further in the field by placing two other devices (SFM_X2 and SFM_TK.D) in a ventilated passage at Milandre Cave, Switzerland. These two instruments were installed on two opposite corners of a 0.68 x 0.68 m trapdoor present in the cave and recorded in parallel for 75 days.

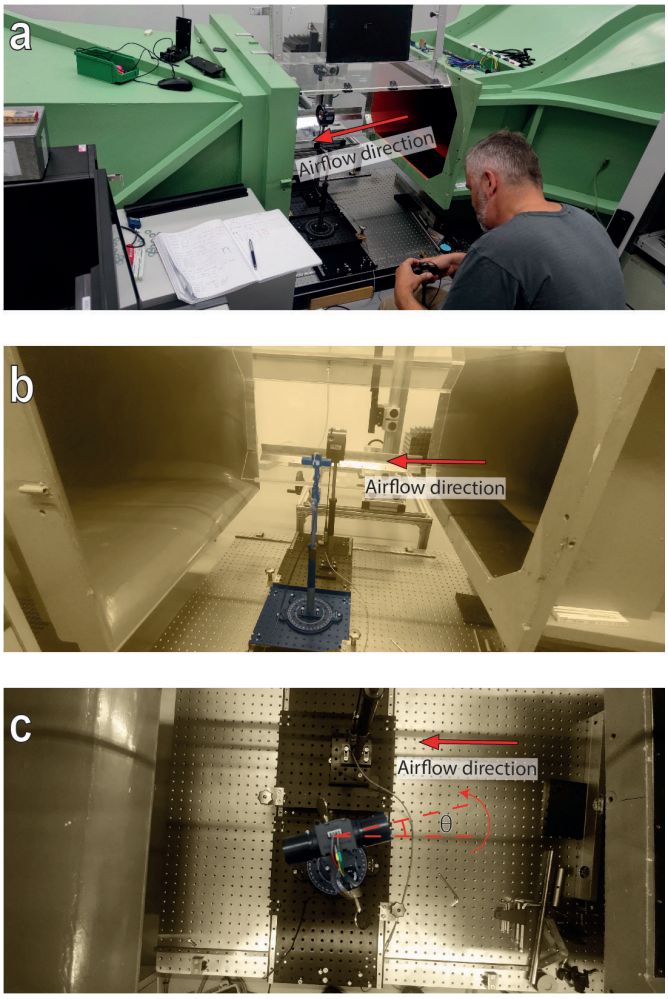

Fig. 2. The METAS' wind tunnel (a), the experimental setup (b) and the rotational experiment (c).

Air velocity distributions across a cave cross-section

The uncertainties related to the wall-air boundary layer were investigated in another ventilated cave (Longeaigue Cave, Val-de-Travers, Switzerland). Longeaigue Cave ventilation is dominated by a chimney effect (Pastore et al., 2024), with a driving pressure strongly related to the temperature difference between inside and outside the cave (Badino, 1995; Lismonde, 2002; Luetscher & Jeannin, 2004). Inside the cave, an irregular cave cross-section was instrumented using three calibrated SFM devices (SFM-1, SFM-2 and SFM_{wall}, Fig. 3). These instruments were deployed simultaneously in the 1.2 m^2 cave passage (1.27 m wide) at a similar height, 0.64 m above ground. One instrument was in direct contact with the cave wall (SFM_{wall}), while the two others (SFM-1 and SFM-2, Fig. 3) were positioned at distances of 0.31 m and 0.54 m from SFM_{wall}, respectively. The experimental setup was left in the cave for one week (6 October – 13 October 2023) with strong diurnal variations including flow reversals (upward and downward ventilation).

Modelling approach and numerical simulation

A 3-D lidar scan (Leica BLK2GO) was made along the 8 m long conduit hosting the SFMs in Longeaigue Cave (Fig. 3). The spatial resolution of the point cloud is up to 5 cm but was reduced to 20 cm during data processing to decrease the computational time of numerical simulations. The conduit is considered far enough from cave entrances such as $T_{wall} \approx T_{air}$ (Sedaghatkish et al., 2024), therefore the effect of free convection on the wall surface is negligible. Figure 4a & b displays the scanned cave passage. The conduit has only two openings, which act alternatively as inlets and outlets, depending on the direction of the airflow. When the airflow is downward, the inlet is at the top of the z-axis and the outlet is at the bottom. For upward flow, the inlet and outlet are reversed. The red cross-section in Figure 4b, at the projected distance y = 5.7 m, highlights the instrumented cross-section (from now on $CS_{5.7m}$).

We developed a numerical model using COMSOL Multiphysics® v6.2 (COMSOL Multiphysics®, 2023) to calculate the velocity components and pressure. The software works based on Finite Element Analysis (FEA) for the discretization of Partial Differential Equations (PDE) by subdividing the computational domain into smaller parts called finite mesh elements.

The governing equations comprise the continuity-momentum equations as well as the k-ε turbulence model based on Reynolds-Averaged Navier-Stokes formulations (RANS). The full form of the equations can be found in Hammoodi et al. (2022) and Sivakumar et al. (2021). The k-ε model solves for two variables: k, the turbulence kinetic energy; and ε, the rate of dissipation of turbulence kinetic energy. More comprehensive explanations about the k-ε turbulence model can be found in Wilcox (1998).

Incompressible and steady-state airflow is considered. A uniform velocity distribution is imposed at the inlet boundary. The atmosphere pressure is imposed at the outlet and a no-slip (zero velocity) boundary condition is employed for the cave walls. The air density and dynamic viscosity are assumed equal to 1.24 kg/m^3 and 1.77 × 10^{-5} Pa·s, respectively.

Mesh independence was tested for different numbers of grid resolutions to finally select a total of 1.78 million elements. The numerical results do not change with increasing mesh elements.

A turbulent flow is verified when Reynolds number (Re) > 2 × 10^3, where $Re = 4Q\rho/\pi d\mu$, Q is the volume flow rate [m^3/s], ρ is the density of humid air (1.24 kg/m^3 at 10°C), d is the aeraulic diameter [m] determined as $4 \cdot area/perimeter$, and μ is the dynamic viscosity of air.

The numerical model provides the air velocity distributions under stationary conditions in a turbulent regime. Although

the comparison with field data may be only qualitative because of steady-state assumption, the model provides a better understanding of the relative position of the instruments in the streamlines and supports the interpretation and quantification of uncertainties derived from complex conduit geometries.

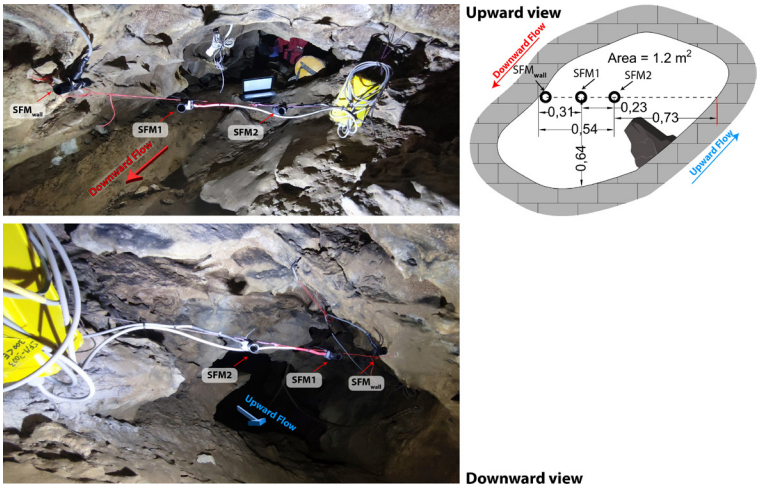

Fig. 3. Position of the instruments to test the velocity distribution in Longeaigue Cave. The dimensions on the right are in meters.

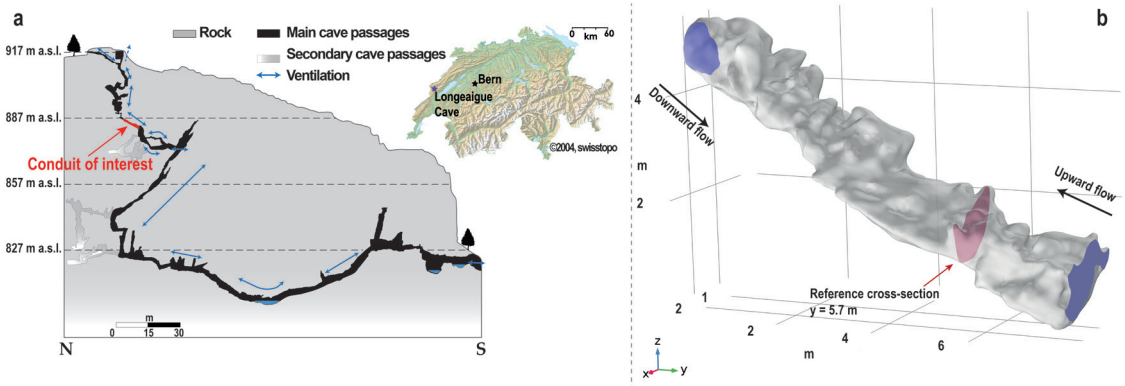

Fig. 4. a) An excerpt of the Longeaigue Cave survey (modified after Jeannin, 2018) and the scanned conduit highlighted in red. b) The computational domain of the 3-D scanned cave passage. Inlet/outlet boundaries are indicated in blue colour. In red is the reference cross-section $CS_{5.7m}$ (y = 5.7 m).

RESULTS

Device calibration and reproducibility

Figure 5 shows the experimental time series measured in the wind tunnel with SFM_SN0708 at 0.5, 1.6, 2.0, and 5.0 m/s. For each velocity, the measured values (in Standard Liter per Minute, SLM) exhibit a standard deviation (σ) in the order of a few per cent (n = 401). The calibration results are given in Table 2 and Figure 6a. The uncertainty is up to 26% for velocities <0.30 m/s, while between 6 and 3% above 0.5 m/s. Table 2 confirms that the SFM flow meter measures almost the same value when rotated by 180° within the airflow. This consistency is also evident in Figure 6a, indicating that the measurements are equally reliable in both directions.

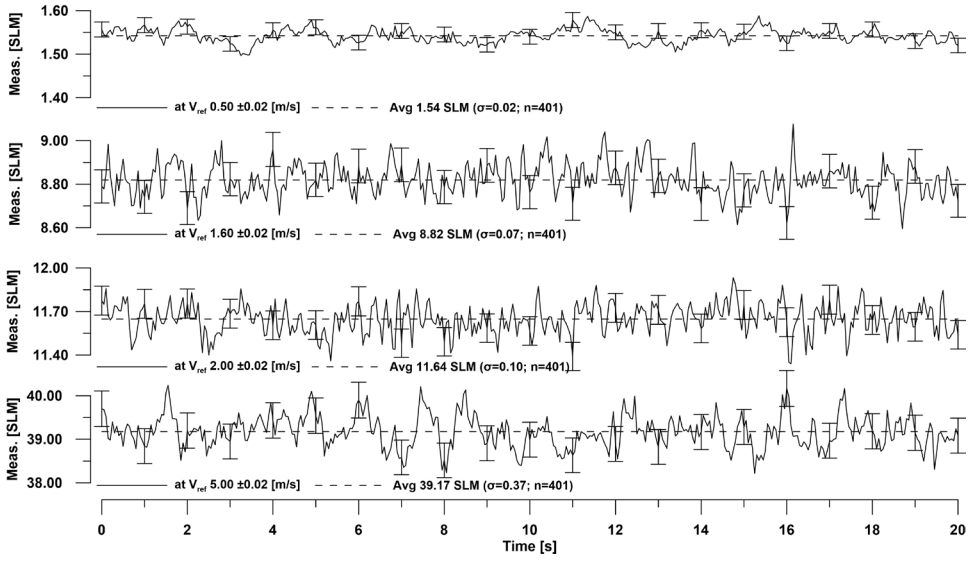

Fig. 5. SFM data series (in standard litre per minute) at four reference velocities (V_{ref} =0.50/1.60/2.00/5.00 m/s). Results show a low standard deviation (σ; n = 401) at constant airflow.

Table 2 – Reference velocities and measured SFM response in standard litre per minute (SLM) at 0° (+values) and 180° (-values).

V_{ref}	Avg_{SLM} at 0°	σ_{SLM}	SFM Err_{abs}	SFM Err_{rel}
(m/s)	**(+SLM)**	**(n = 401)**	**(m/s)**	**(%)**
0.15 (±0.02)	0.19	0.008	0.04	26%
0.30 (±0.02)	0.61	0.015	0.03	10%
0.50 (±0.02)	1.54	0.017	0.03	6%
0.80 (±0.02)	3.33	0.035	0.04	5%
1.20 (±2%)	5.94	0.054	0.04	3%
1.60 (±2%)	8.81	0.077	0.05	3%
2.00 (±2%)	11.66	0.099	0.07	4%
2.50 (±2%)	15.94	0.156	0.08	3%
3.00 (±2%)	20.44	0.165	0.09	3%
5.00 (±2%)	39.28	0.405	0.16	3%
8.00(±2%)	73.84	1.095	0.3	4%
V_{ref}	Avg_{SLM} at 180°	σ_{SLM}	SFM Err_{abs}	SFM Err_{rel}
(m/s)	**(-SLM)**	**(n = 401)**	**(m/s)**	**(%)**
0.14 (±0.02)	-0.15	0.014	0.04	28%
0.30 (±0.02)	-0.6	0.018	0.04	13%
0.50 (±0.02)	-1.5	0.02	0.03	6%
0.80 (±0.02)	-3.37	0.039	0.04	5%
1.60 (±2%)	-9.12	0.087	0.06	4%
2.50 (±2%)	-16.02	0.15	0.08	3%

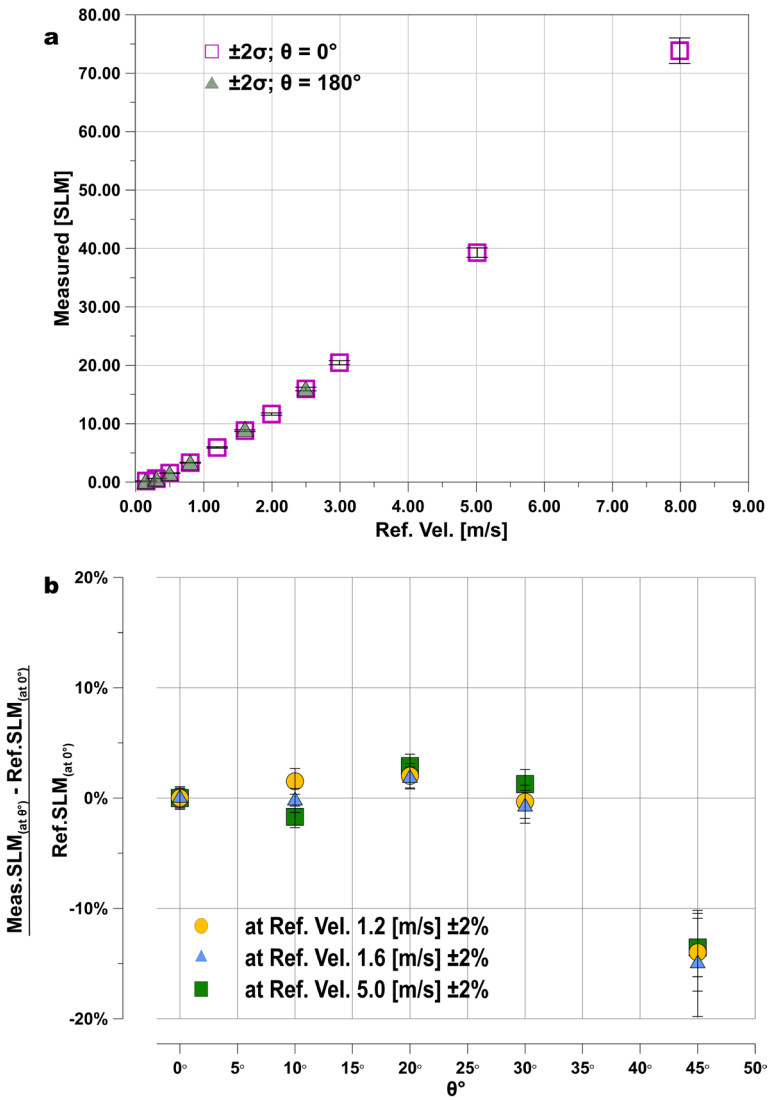

Fig. 6. a) Measured SLM (y-axis) against the reference velocities (x-axis). b) Rotation test results at three V_{ref}. For 0°<θ<30° and 1.2<V_{ref}< 5.0 m/s, the velocity deviation from reference is reasonably low (between 0.33% and 3%). For θ = 45°, the deviation exceeds 10% for all the velocities.

The rotation experiment (Fig. 6b) shows that with angles within 10° to 30° from the flow axis, the deviation of the SFM measurements ($SLM_{(at\ \theta°)}$ – $Ref.SLM_{(at\ 0°)}$ / $Ref.SLM_{(at\ 0°)}$) ranges between 0.33% and 3% for V_{ref} values between 1.2 and 5.0 m/s. At 45°, the error exceeds 10% for all the velocity steps. These results indicate that the pressure drops associated with the instrument shape and orientation are not significant as long as the angle stays reasonably low (less than 30°).

The SFM_SN0708 calibrated in the wind tunnel was compared with the other two SFMs (SFM-1_SN0501 and SFM-2_SN0382) tested in the SISKA's lab using the pipe with a fan. Results are shown in Figure 7a. The values are well correlated with a ratio close to 1:1 compared to the reference SFM_SN0708. The high standard deviation evident in Figure 7a is rather due to the flow instability along the pipe than to instrument deviation, showing that measurements should last sufficiently long to compensate for such turbulent fluctuations.

The devices setup in Milandre Cave (SFM_X2 and SFM_TK.D) also confirm the instrumental reproducibility (Fig. 7b).

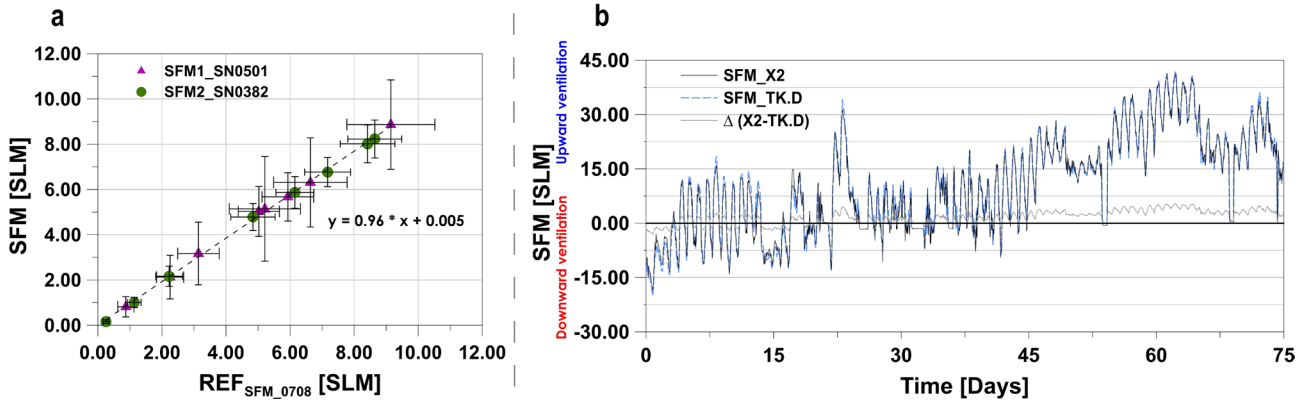

Fig. 7. a) Comparison between SFM-1 and SFM-2 using a pipe with a fan. Results highlight the reproducibility of the two instruments. b) Comparison between SFM_X2 and TK.D at the trapdoor in Milandre Cave. These results confirm the reproducibility of the instruments.

Cave monitoring

Figure 8 shows the measurements from three different SFMs deployed in the same cross-section in Longeaigue Cave, close to and far from the cave wall. The hourly time series show clear differences between the instruments (Fig. 8). SFM-1, located at 0.31 m from one wall and 0.96 m from the other, measured the highest velocities in both ventilation regimes (1.39 ±0.07 m/s;-1.00 ±0.04 m/s). SFM_{wall} measured velocities close to SFM-1 during upward flow. Instead, SFM-2, located at 0.54 m and 0.73 m from the walls, logged velocities close to SFM_{wall} during the downward ventilation (+velocities), and comparable to SFM-1 during the upward ventilation (-velocities).

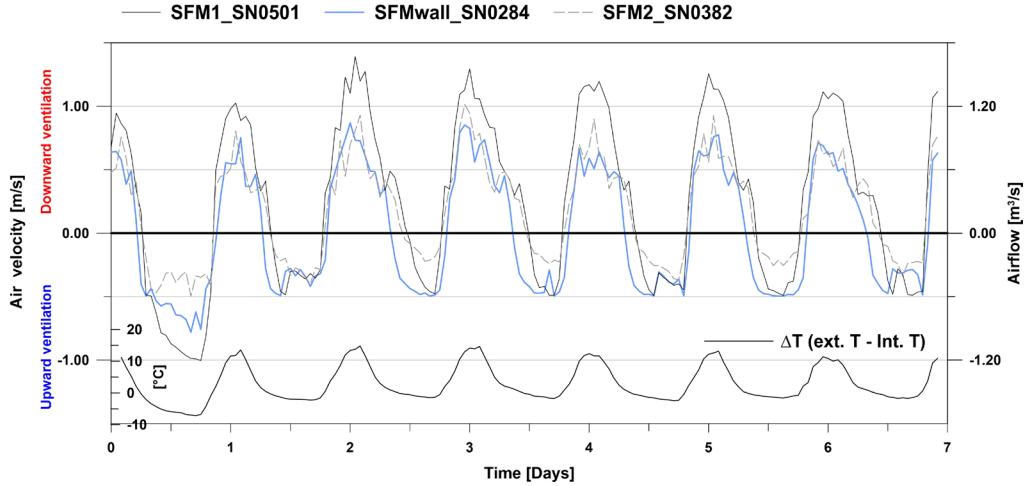

Fig. 8. Diurnal ventilation cycles of cave air velocities measured with SFM-1, SFM-2, and SFM_{wall} in the same cross-section at an hourly time step. The data were recorded in Longeaigue Cave (Switzerland) between 06 October and 13 October 2023. The lower part of the graph shows the ΔT (°C) between the external temperature measured in front of the cave entrance and the cave temperature at the same location as the SFMs.

Modelled air velocities

The simulations were carried out with steady airflows of 0.65, 1.35, and 2.00 m^3/s, for both upward and downward flows. These airflow values were chosen based on field observations (Pastore et al., 2024) and cover most of the spectrum of possible airflows in Longeaigue Cave. The model results (Fig. 9) are compared with empirical data measured in a cross-section at 5.7 m (projected distances on the y-axis) from the upper end of the conduit ($CS_{5.7m}$). The measured velocities confirm a turbulent regime with a Reynolds number ranging between 10^4 and 10^5.

The velocity distributions modelled for an airflow of 1.35 m^3/s are shown in Figure 9a, b for cross-sections at 2.2 m, 3.5 m (projected distances on the y-axis), and $CS_{5.7m}$. The model results clearly show that the velocity distribution depends on the 3-D geometries

and flow direction: while for downward flow low-speed zones appear to be more prominent near the ceiling in the 3.5 m and $CS_{5.7m}$ cross-sections, such zones are visible on the right wall (from an upward point of view) during upward flow. At the cross-section 2.2 m the presence of an obstacle reduces the speed at the floor for the downward-modelled flow.

Focusing on $CS_{5.7m}$, the results for the three modelled airflows are shown in Figure 9c-h. For low airflow (Fig. 9c and f with 0.65 m^3/s) we observe a quite homogenous distribution of velocities (between 0 and 1 m/s) compared to higher airflows (0 – 3 m/s). The velocity distribution within the cross-section is also different depending on the airflow direction: a zone of low velocity is more expanded in the top-right corner for all upward models(Fig. 9f-h) than for downward models. This low-speed zone is due to the presence of a rock chock visible in the 3-D scan and in Figure 3 (downward view). For all airflows, the centre-low of the cross-section always displays the highest velocities (Fig. 9).

In Figure 9, the position of the SFM probes is depicted. Downward velocities from SFM-1, SFM-2, and SFM_{wall} can be compared with velocity distributions predicted for 1.35 m^3/s downward airflow (Fig. 9d). For this flow rate, modelled velocity distributions show higher values at SFM-1 than at SFM_{wall} as observed in situ (Fig. 8). However, the model predicts a higher velocity at SFM-2 than at SFM-1 and SFM_{wall}, which contrasts with the higher velocities measured at SFM-1 during downward ventilation (Fig. 8).

During upward ventilation, measured velocities (Fig. 8) compare well with the modelled velocities for 0.65 m^3/s (Fig. 9f). Both, the measured (dashed line in Fig. 8) and predicted velocities of SFM-2 show lower values than SFM-1 and SFM_{wall}.

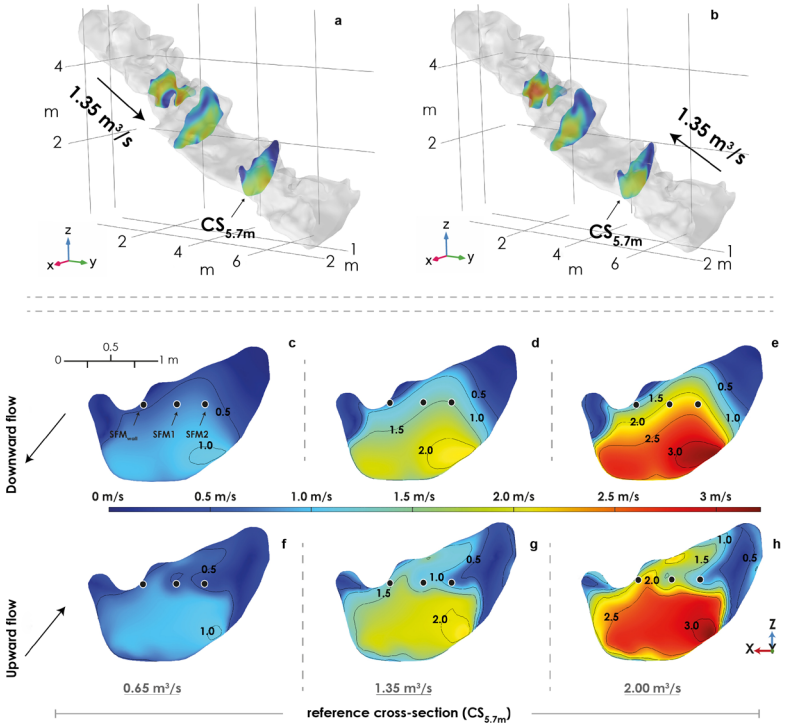

Fig. 9. Modelled air velocity distributions along the conduit and at the same cross-section as the cave measurements. $CS_{5.7m}$ velocities refer to three different airflows and opposite flow directions. The three black circles identify the SFM positions as deployed in the cave.

DISCUSSION

Quality of the measurements and airspeed conversion

Flow measurements under steady conditions in an air tunnel showed a high precision of the SFM (±1%) between 0.5 and 5 m/s (Table 2, Fig. 5 and Fig. 6a). The 17 individual measurements (Fig. 6a) show an instrumental uncertainty Err_{rel} of ±5% between 0.5 and 8 m/s, and between 26/28% and 10% for 0.15 $<V_{ref}<$ 0.5 m/s, for both flow directions. Nevertheless, turbulent flow is typical for caves (Lismonde, 2002) where the spatial variability of the cross-section can be significant, leading to an increase in the Reynolds number (*Re* >> 2000). Thus, in a turbulent field, the stochastic error related to the sampling may impact the measurements (Mauder and Zeeman, 2018; Finkelstein & Sims, 2001).

The data is reproducible (Fig. 7a and b) and non-sensitive to minor changes in orientation (3% at θ = 30°; Fig. 6b) making it suitable for installation in complex cave sections. The device proved to measure correctly in both directions, a requirement that fits well with the dual behaviour of a cave ventilated by a chimney effect.

The relationship between measurements (V_{ref} against SLM) shown in Figure 6a was found to be close to quadratic. Although the relation between mass flow rate and temperature difference in a thermal flowmeter is first-order (i.e., linear), other thermal processes may compete for a non-linear relationship (e.g., thermal exchanges with device walls). In particular, the device is designed to measure in a closed system with a pipe as a flow inlet. Instead, we deploy the instrument immersed in a flow that is free to enter the pipe device, thus probably causing boundary effects of the second order that may disrupt linearity.

The conversion of SLM into m/s can be derived by plotting the points shown in Figure 6a with the two axes swapped (x-axis = SLM and y-axis = m/s). Depending on the interested velocity range, it is possible to fit the equation for the desired V_{ref} range. In the case of Milandre (Fig. 7b) and Longeaigue (Fig. 8), we aimed to apply the conversion within the range of $0 \leq |SLM| \leq 39.0$ ($0 \leq |V| \leq$ ~5.0 m/s), ensuring that the intercept of the equation is forced to 0 (i.e., 0 m/s = 0 SLM). Since a single equation would not fit within 2σ for SLM≤ 6.0 (~|V|≤ 1.2 m/s), thereby increasing the relative error at low speeds, two different equations were obtained.

Within the range $6.0 \leq |SLM| \leq 39.0$ (~$1.2 \leq |V| \leq$ ~5.0 m/s), the conversion is obtained by Eq. 1:

$$y = -0.0014 \cdot x^2 + 0.1828 \cdot x$$

while for $6.0 \leq |SLM|$ ($|V| \leq$ ~1.2 m/s) by Eq. 2:

$$y = -0.0243 \cdot x^2 + 0.3422 \cdot x$$

The velocity absolute value assures the same equation for both flow directions (positive or negative). The original measurement sign (indicating the flow direction) can be restored after the conversion into meters/second.

According to the manufacturer, no corrections for either barometric pressure or temperature are needed.

Airspeed distribution through a cross-section

The high reproducibility of the instruments allows for studying the impact of conduit geometries on the measured air velocity (Fig. 3 and Fig. 8). The comparison of the values measured by three different SFM sensors within the same cross-section of a cave passage pointed out differences, which are clearly beyond the range of the instrument accuracy. This reflects the heterogeneity of the flow field within the cave cross-section. At the test site, SFM-1 measured the highest velocities during the experiment (Fig. 8). This is likely due to the SFM-1 position in a sort of "channel" free of obstacles, as shown in Figure 3. SFM_{wall} did not show the lowest velocities, despite being located on the wall. Instead, the lowest velocities were measured at SFM-2 during the upward regime (negative values) although the instrument was far from the walls (0.54 m and 0.73 m). Therefore, SFM-2 exhibits a different response during downward and upward ventilation, when compared with SFM-1. This is probably due to the presence of an obstacle affecting the flow, causing a different response according to the wind direction. We conclude that the position of the SFM-1 is less affected by the cross-section morphology since it measured the highest velocities. During downward regimes (+val.), the velocity difference between SFM-2 and SFM-1 (taken as a reference) is -42% as well as between SFM-1 and SFM_{wall}. Conversely, in the upward regimes, the velocity difference between SFM-1 and SFM_{wall} reduces to approximately -21%, while staying at -42% for SFM-2.

The airflow modelled along the 3-D conduit geometry confirms the results obtained from field measurements. In fact, the modelled velocities highlight the spatial variability along the conduit (Fig. 9). These differences are related to the complex geometry of the conduit and the distribution of the obstacles therein (Fig. 9a, b). Furthermore, airspeed distributions are less uniform across $CS_{5.7m}$ as airflow increases. Consequently, the differences measured between the three SFMs can sensibly increase at a high volumetric flow rate. The flow distribution changes also according to the flow direction, as shown by the low-speed zone appearing during upward flow. Nevertheless, the model prediction contrasts with SFM-2 field measurements during downward flow, since the model predicted higher velocity than SFM-1. The reduction of the 3-D resolution (from 5 to 20 cm) and the associated loss in spatial resolution could explain a different velocity distribution. Our results show that the measurement of the air velocity in natural settings (e.g. a cave) depends not only on the airflow but also on the relative position of the instrument in the streamlines and flow direction.

Impact on air volume estimation

Long airflow data series in caves are of interest to study the air dynamics (Faimon & Lang, 2013; Gomell & Pflitsch, 2022) and the associated energy exchanged therein (Luetscher et al., 2008; Obleitner & Spötl, 2011). Airflow monitoring derives usually from a punctual airspeed measurement integrated through a specific cross-section, but this may not necessarily represent the average velocity across the entire cross-section. The instrument position determines the measured velocities and these uncertainties impact the calculated airflow (m^3/s) distributed over the 1.2 m^2 $CS_{5.7m}$ (Fig. 8 and Fig. 9c-h). Instruments placed in the same cross-section have shown differences as high as 42% (~0.5 m/s) between them, although they were only a few dozen centimeters away from each other. These experimental data were confirmed by modelled air velocity distribution in a cave cross-section.

The modelled air distributions suggest that there is no clear location to deploy a single anemometer within a cross-section (Fig. 9). If an anemometer is placed in a high-speed zone, there is a high possibility of overestimating the airflow. Conversely, positioning it close to the wall may result in an underestimation of the flow. The model in Figure 9 suggests that the average velocity between SFM-1, SFM-2, and the SFM_{wall} position is likely to provide a value close to the actual airflow rate. For instance, considering velocities of 0.6, 1.3, and 1.5 m/s for SFM_{wall}, SFM-1, and SFM-2, respectively, results in an airflow rate of 1.4 m^3/s over the $CS_{5.7m}$ (1.2 m^2). This value closely matches the modelled 1.35 m^3/s. Therefore, the actual airflow passing through $CS_{5.7m}$ during the monitored period is likely to average the airflows measured at SFM-1, SFM-2, and SFM_{wall}.

The cumulated air volume transiting through Longeaigue Cave over seven days is shown in Figure 10 for the three devices. As expected from the airspeed time series (Fig. 8), the total air volume integrated with SFM-1 values is the highest with $4.4 \cdot 10^5$ m^3 (~$5.4 \cdot 10^5$ kg). It overtakes the air volumes measured by SFM-2 and SFM_{wall} by 39% and 27%, respectively. Since the estimation of the air volume passing through $CS_{5.7m}$ is directly dependent on the inferred airflow, the average air volume estimated from the three instruments should provide a good approximation

of the total air volume over the monitored period (Fig. 10, dashed orange line). Moreover, the three cumulated curves in Figure 10 show different slopes, but also vary according to the flow direction (coloured arrows). The latter indicates that the driving pressure related to the ΔT (external – internal temperature, Fig. 8) did not act symmetrically on the system during the monitored days: the temperature difference was higher during the day (downward ventilation) than at night (upward ventilation). During downward flow, the slopes highlighted by blue arrows in Figure 10 are steeper than during upward ventilation (green arrows), implying that $Vol_{downward} >> Vol_{upward}$ for SFM-1 and SFM-2. SFM_{wall}, on the other hand, displayed $Vol_{downward} \approx Vol_{upward}$.

These results show clearly that the positioning of the instrument plays an important role in the measurement uncertainties. In our case, these uncertainties largely dominate the instrument uncertainty (±5%) and those related to the device's orientation (2.5% at 1.2 m/s, ±20°). Therefore, choosing the appropriate measurement point is not straightforward. Depending on the researched precision, more than one flowmeter should be deployed in a single cross-section to infer an average air velocity to be integrated over the cross-section. However, if only one instrument is to be used, the measuring point could be chosen after carrying out manual measurements with a hand-held anemometer to investigate the velocity distribution (taking care to cover the whole cross-section, and not to disturb the flowfield by the human body within or close to the cross-section). A fixed anemometer should not be deployed in the high-speed zone nor the low-speed zone, but in a velocity field which could represent as closely as possible the average velocity. In the case of one-time measurements to estimate airflow with a hand-held anemometer, one approach could be to measure airflow in three or more different cross-sections along the same conduit. The volumetric airflow derived from measurements with anemometers (hand-held or in place) may also be compared with tracer gauging tests (Pastore et al., 2024). In fact, the latter does not require velocity integration, as it is derived from the mass conservation equation and yields reliable flow rates even at low air speeds.

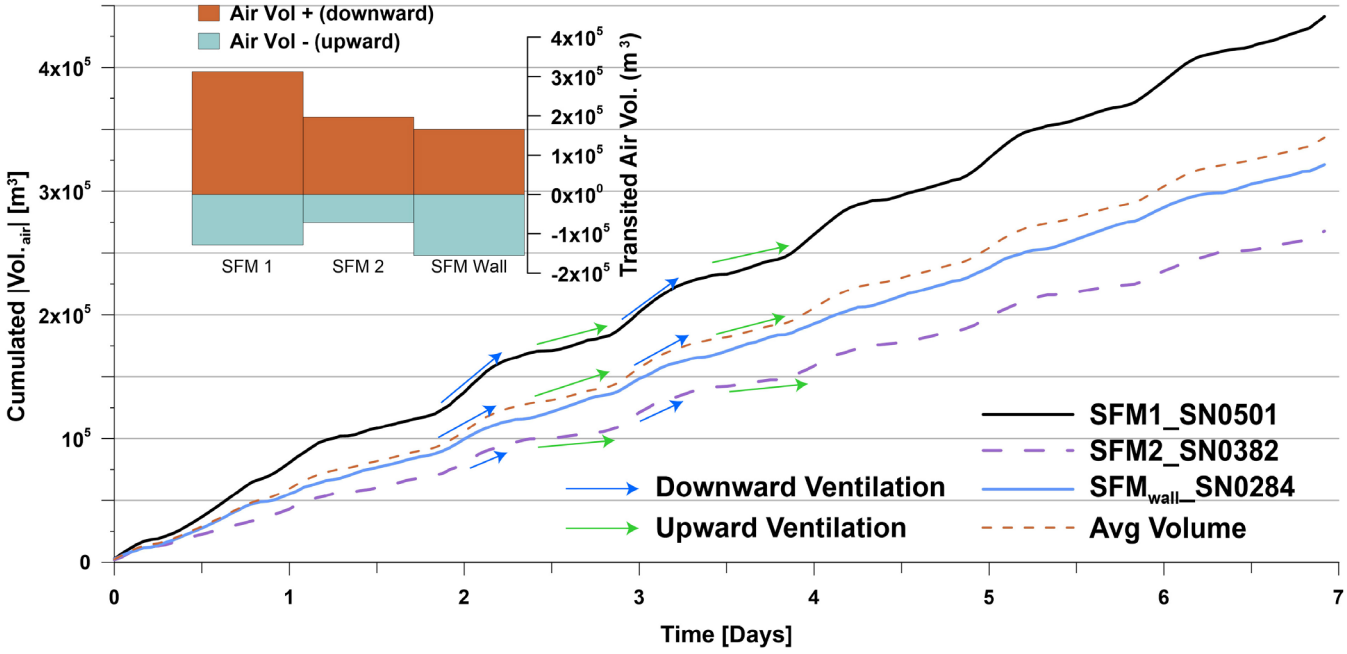

Fig. 10. Cumulated air volumes evaluated from the data series shown in Figure 8.

Experience from long-term monitoring

The testing of SFM probes in a wind tunnel, in the SISKA's lab with a pipe and in naturally ventilated conduits, revealed these probes to be suitable for cave monitoring, more than most other types of sensors we tested. Several SFMs were installed for at least one year in different caves subject to chimney ventilation. Some of these data have already been used in scientific publications (Garagnon et al., 2022; Sedaghatkish et al., 2024). Furthermore, three years of airflow monitoring data (very few gaps) collected with an SFM device in Longeaigue Cave are being interpreted to assess air thermal exchanges within the ventilated conduits. Despite environmental conditions including high-condensing environments, freezing conditions, sporadic flooding, and anthropogenic disturbances, the instruments have measured with high reliability, confirming their robustness. In our experience, most of the acquisition gaps did not derive from the sensor, but from the failure of the logger's electronic parts, more sensitive to environmental conditions, or battery failures. Good insulation of electronic parts is, therefore, a priority. The battery duration depends on the efficiency of the logging system since the device itself requires only 3.3 V to run (~3.8 mA during measurements). For instance, in D7.1 Cave (Switzerland) we deployed an SFM working with our logger based on a TinyPICO microcontroller appropriately coded and powered by a 3.7 V/5500 mAh lithium battery. This cave is difficult to access (high mountain cave), so we left the instrument working for 1 year with a 1 hour time step and without any maintenance (Sedaghatkish et al., 2024). However, after prolonged exposure,

condensation within the SFM pipe could potentially disrupt measurements. Our field experience indicates that installing the device with the electronic sensing part (Fig. 1) upside down allows moisture to drip away from the sensor. In any case, after drying the sensor (e.g. with a light cloth), the device usually worked again. This positive experience with the SFM contrasts with independent measurements carried out with various other commercial devices, including an ultrasonic anemometer, which could not handle the condensing conditions without extra heating, possibly affecting the cave climate locally, and which would require an additional power supply.

CONCLUSIONS

Measuring airflows in caves is of interest to study the air dynamics and the related energy exchanges in karst systems. Besides reliable measurements, high-performance and robust instruments are key points when investigating challenging environments such as caves. In this article, we tested an instrument that meets our requirements: 1) low power supply, 2) reliable measurements, 3) durability, and 4) affordability. The instrument showed a low Err_{rel}, ± 5% between 0.5 and 5 m/s, a high resolution (up to 16 bit) and the indication of flow direction. Nevertheless, despite the high resolution and accuracy of the instrument, calculating the volume or mass flow rates from air velocity measurements might be not obvious. This difficulty arises primarily because the velocity field within a single cross-section is non-uniform and fluctuates with the flow rate and direction.

Our results show clearly that the position of a single instrument in a cave conduit plays a major role in the estimation of the airflow. While long-term monitoring with single instruments unlikely records the “real” airflow, determining a plausible range of airflow is key for the calculation of energy balances or the modelling of aerosol transport. Airflow monitoring with several instruments distributed in the same cross-section could help to reduce the measurement uncertainty. Computational models aiming to correct the integration of one-point velocity measurement in a specific cross-section represent another possible approach.

ACKNOWLEDGEMENTS

The authors would like to acknowledge Tanguy Racine (Université de Neuchâtel) for carrying out the 3-D lidar scan in Longeaigue Cave. We also thank Dr. M. de Huu from METAS, who provided the airflow calibration in the wind tunnel. This work was funded by the Swiss National Science Foundation (SNSF) [200021_188636].

Authorship statement: CP, ML, and PYJ designed and directed the study. EW and NS developed the electronic devices used for the measurements. CP performed the measurements and analyzed the field data. AS carried out the simulations. CP wrote the paper with input from all authors.

REFERENCES

Badino, G., 1995. Fisica del clima sotterraneo, Memorie dell'Istituto Italiano di Speleologia. Società Speleologica Italiana, Vol. 7, 144 p.

Breecker, D.O., Payne, A.E., Quade, J., Banner, J.L., Ball, C.E., Meyer, K.W., Cowan, B.D., 2012. The sources and sinks of CO_2 in caves under mixed woodland and grassland vegetation. Geochimica et Cosmochimica Acta, 96, 230-246. https://doi.org/10.1016/j.gca.2012.08.023

COMSOL Multiphysics®, 2023. CFD Module User's Guide v6.2 [WWW Document]. URL https://doc.comsol.com/6.2/docserver/#!/com.comsol.help.comsol/helpdesk/helpdesk.html (accessed 4.30.24).

Dominguez-Moñino, I., Jurado, V., Rogerio-Candelera, M.A., Hermosin, B., Saiz-Jimenez, C., 2021. Airborne bacteria in show caves from Southern Spain. Microbial Cell, 8(10), 247-255. https://doi.org/10.15698/mic2021.10.762

Faimon, J., Lang, M., 2013. Variances in airflows during different ventilation modes in a dynamic U-shaped cave. International Journal of Speleology, 42(2), 115-122. https://doi.org/10.5038/1827-806X.42.2.3

Fan, H.B., Liu, J.L., Sun, G.Z., 2018. Design of low-power ultrasonic anemometer based on STM32L476. IOP Conference Series: Materials Scientific Engineering, 408, 012036. https://doi.org/10.1088/1757-899X/408/1/012036

Finkelstein, P.L., Sims, P.F., 2001. Sampling error in eddy correlation flux measurements. Journal of Geophysical Research, 106(D4), 3503-3509. https://doi.org/10.1029/2000JD900731

Gabrovšek, F., 2023. How do caves breathe: The airflow patterns in karst underground. PLoS ONE, 18, e0283767. https://doi.org/10.1371/journal.pone.0283767

Garagnon, J., Luetscher, M., Weber, E., 2022. Ventilation regime in a karstic system (Milandre Cave, Switzerland). Proceedings of the 18th International Congress of Speleology, 3, 187-190. https://hal.science/hal-03932677

George, D.S., Rao, S.N., Bennaceur, K., 2018. A survey of ultrasonic anemometers. In: 2018 IEEE International Conference on Computational Intelligence and Computing Research (ICCIC), IEEE, Madurai, India, p. 1-4. https://doi.org/10.1109/ICCIC.2018.8782390

Hammoodi, K.A., Hasan, H.A., Abed, M.H., Basem, A., Al-Tajer, A.M., 2022. Control of heat transfer in circular channels using oblique triangular ribs. Results in Engineering, 15, 100471. https://doi.org/10.1016/j.rineng.2022.100471

Jeannin, P.-Y., 2018. La Baume de Longeaigue, 30 ans de silence. Cavernes, 32-49.

Jeannin, P.Y., Malard, A., Häuselmann, P., Meury, P.X., 2017. Effect of cave ventilation on karst water chemographs. Proceeding of the Eurokarst 2016 Conference, Neuchâtel, Switzerland, September 2016. p. 129-139. https://doi.org/10.1007/978-3-319-45465-8_14

Kowalczk, A., Froelich, P., 2010. Cave air ventilation and CO_2 outgassing by radon-222 modeling: How fast do caves breathe? Earth and Planetary Science Letters, 289(1-2), 209-219. https://doi.org/10.1016/j.epsl.2009.11.010

Kukuljan, L., Gabrovsek, F., Covington, M., 2021. The relative importance of wind-driven and chimney effect cave ventilation: Observations in Postojna Cave (Slovenia). International Journal of Speleology, 50(2), 275-288.

https://doi.org/10.5038/1827-806X.50.3.2392
Leoni, A., Stornelli, V., Pantoli, L., 2018. A low-cost portable spherical directional anemometer for fixed points measurement. Sensors and Actuators A: Physical, 280, 543-551. https://doi.org/10.1016/j.sna.2018.08.025
Lismonde, B., 2002. Climatologie du monde souterrain. Tome 2: Aérologie des systèmes karstiques. Comité Départemental de Spéléologie de l'Isère.
Luetscher, M., Jeannin, P.Y., 2004. Temperature distribution in karst systems: the role of air and water fluxes. Terra Nova, 16(6), 344-350. https://doi.org/10.1111/j.1365-3121.2004.00572.x
Luetscher, M., Lismonde, B., Jeannin, P.-Y., 2008. Heat exchanges in the heterothermic zone of a karst system: Monlesi cave, Swiss Jura Mountains. Journal of Geophysical Research, 113(F2). https://doi.org/10.1029/2007JF000892
Martin-Pozas, T., Cuezva, S., Fernandez-Cortes, A., Cañaveras, J.C., Benavente, D., Jurado, V., Saiz-Jimenez, C., Janssens, I., Seijas, N., Sanchez-Moral, S., 2022. Role of subterranean microbiota in the carbon cycle and greenhouse gas dynamics. Science of the Total Environment, 831, 154921. https://doi.org/10.1016/j.scitotenv.2022.154921
Mauder, M., Zeeman, M.J., 2018. Field intercomparison of prevailing sonic anemometers. Atmospheric Measurement Techniques, 11(1), 249-263. https://doi.org/10.5194/amt-11-249-2018
Medina, M.J., Antić, D., Borges, P.A.V., Borko, Š., Fišer, C., Lauritzen, S.-E., Martín, J.L., Oromí, P., Pavlek, M., Premate, E., Puliafico, K.P., Sendra, A., Reboleira, A.S.P.S., 2023. Temperature variation in caves and its significance for subterranean ecosystems. Scientific Reports, 13(20735). https://doi.org/10.1038/s41598-023-48014-7
Monitaro, M., Domanski, K., 2023. Thermal-mass measurement principle: The best choice for hydrogen-ready gas meters [WWW Document]. Sensirion - Specialist Articles. URL https://sensirion.com/products/product-insights/specialist-articles/thermal-mass-measurement-principle [accessed 11.10.23].
Obleitner, F., Spötl, C., 2011. The mass and energy balance of ice within the Eisriesenwelt cave, Austria. The Cryosphere, 5(1), 245-257. https://doi.org/10.5194/tc-5-245-2011
Pastore, C., Weber, E., Doumenc, F., Jeannin, P.-Y., Lütscher, M., 2024. Dispersion of artificial tracers in ventilated caves. International Journal of Speleology, 53(1), 51-62. https://doi.org/10.5038/1827-806X.53.1.2497
Prelovšek, M., Šebela, S., Turk, J., 2018. Carbon dioxide in Postojna Cave (Slovenia): spatial distribution, seasonal dynamics and evaluation of plausible sources and sinks. Environmental Earth Science, 77, 289. https://doi.org/10.1007/s12665-018-7459-6
Sedaghatkish, A., Pastore, C., Doumenc, F., Jeannin, P.-Y., Luetscher, M., 2024. Modeling heat transfer for assessing the convection length in ventilated caves. Journal of Geophysical Research: Earth Surface, 129, e2024JF007646. https://doi. org/10.1029/2024JF007646
Sensirion®, 2024. SEK-Control Center [WWW Document]. URL https://www.sensirion.com/products/sensor-evaluation/control-center [accessed 5.4.24].
Sivakumar, K., Kumar, T.S., Sivasankar, S., Ranjithkumar, V., Ponshanmugakumar, A., 2021. Effect of rib arrangements on the flow pattern and heat transfer in internally ribbed rectangular divergent channels. Materials Today: Proceedings, 46, 3379-3385. https://doi.org/10.1016/j.matpr.2020.11.548
Spötl, C., Fairchild, I.J., Tooth, A.F., 2005. Cave air control on dripwater geochemistry, Obir Caves (Austria): Implications for speleothem deposition in dynamically ventilated caves. Geochimica et Cosmochimica Acta, 69(10), 2451-2468. https://doi.org/10.1016/j.gca.2004.12.009
Wang, F., Duan, Y., Lu, M., Zhang, Y., Jing, Z., Sun, C., Peng, W., 2021. Fiber-optic hot-wire anemometer with directional response based on symmetry-breaking induced heat transfer mechanism. Journal of Lightwave Technology, 39(12), 3919-3925. https://doi.org/10.1109/JLT.2020.3015240
Wilcox, D.C., 1998. Turbulence modeling for CFD. DCW industries, La Cañada, CA. ISBN 978-1-928729-08-2.